Please cite this article in press as: Kaneko et al., New Neurons Clear the Path of Astrocytic Processes for Their Rapid Migration in the Adult Brain, Neuron (2010), doi:10.1016/j.neuron.2010.06.018

Neuron
Article

New Neurons Clear the Path of Astrocytic Processes for Their Rapid Migration in the Adult Brain

Naoko Kaneko,[1] Oscar Marín,[2] Masato Koike,[3] Yuki Hirota,[1] Yasuo Uchiyama,[3] Jane Y. Wu,[4] Qiang Lu,[5] Marc Tessier-Lavigne,[6] Arturo Alvarez-Buylla,[7] Hideyuki Okano,[8] John L.R. Rubenstein,[9] and Kazunobu Sawamoto[1,*]
[1]Department of Developmental and Regenerative Biology, Institute of Molecular Medicine, Nagoya City University Graduate School of Medical Sciences, Nagoya, Aichi, 467-8601, Japan
[2]Instituto de Neurociencias, Consejo Superior de Investigaciones Científicas and Universidad Miguel Hernández, Sant Joan d'Alcant 03550, Alicante, Spain
[3]Department of Cell Biology and Neuroscience, Juntendo University Graduate School of Medicine, Bunkyo-ku, Tokyo, 113-0033, Japan
[4]Department of Neurology and Center for Genetic Medicine, Northwestern University Feinberg School of Medicine, Chicago IL, 60611, USA
[5]Division of Neuroscience, Beckman Research Institute of the City of Hope, Duarte, CA 81657, USA
[6]Genentech, South San Francisco, CA 94080, USA
[7]Department of Neurological Surgery and Institute for Regeneration Medicine, University of California at San Francisco, San Francisco, CA 94143, USA
[8]Department of Physiology, Keio University School of Medicine, Shinjyuku-ku, Tokyo, 160-8582, Japan
[9]Nina Ireland Laboratory of Developmental Neurobiology, Center for Neurobiology and Psychiatry, University of California at San Francisco, San Francisco, CA 94143, USA
*Correspondence: sawamoto@med.nagoya-cu.ac.jp
DOI 10.1016/j.neuron.2010.06.018

SUMMARY

In the long-range neuronal migration of adult mammals, young neurons travel from the subventricular zone to the olfactory bulb, a long journey (millimeters to centimeters, depending on the species). How can these neurons migrate through the dense meshwork of neuronal and glial processes of the adult brain parenchyma? Previous studies indicate that young neurons achieve this by migrating in chains through astrocytic tunnels. Here, we report that young migrating neurons actively control the formation and maintenance of their own migration route. New neurons secrete the diffusible protein Slit1, whose receptor, Robo, is expressed on astrocytes. We show that the Slit-Robo pathway is required for morphologic and organizational changes in astrocytes that result in the formation and maintenance of the astrocytic tunnels. Through this neuron-glia interaction, the new neurons regulate the formation of the astrocytic meshwork that is needed to enable their rapid and directional migration in adult brain.

INTRODUCTION

In the developing brain, immature neurons are produced in specific brain regions and migrate to their final destinations, where they assume their mature neuronal functions. Previous studies have established that this process is controlled by various extracellular signals in the neurons' surroundings that are mediated by transmembrane receptors expressed on the migrating neurons (Hatten, 2002; Marín and Rubenstein, 2003). However, little is known about the role migrating neurons may play in the formation and maintenance of their own migration route.

In the adult brain, new neurons are continuously generated in the subventricular zone (SVZ) at the lateral walls of the lateral ventricles, and they migrate into the olfactory bulb (OB), located at the anterior tip of the telencephalon. Throughout life, newly generated immature neurons migrate through the rostral migratory stream (RMS), the pathway leading to the OB (Doetsch and Alvarez-Buylla, 1996; Jankovski and Sotelo, 1996; Lois and Alvarez-Buylla, 1994; Petreanu and Alvarez-Buylla, 2002). How can these neurons migrate through the dense meshwork of neuronal and glial processes of the adult brain parenchyma? During migration, the neurons in the RMS are unipolar or bipolar, with extended leading and trailing processes, and they form elongated cell aggregates called "chains," within which they move over and past one another. The chains of neurons move inside tunnels formed by astrocytic processes, referred to as "glial tubes" (Jankovski and Sotelo, 1996; Kaneko and Sawamoto, 2009; Lois et al., 1996; Okano and Sawamoto, 2008). In several lines of mutant mice, aberrant astrocytic-tube formation is accompanied by a disruption in new-neuron chain migration (Anton et al., 2004; Belvindrah et al., 2007; Chazal et al., 2000; Ghashghaei et al., 2006), suggesting that efficient neuronal migration in the adult brain depends on interactions between the neurons and the astrocytic tubes. Some of these interactions are known. For example, the astrocytes in the RMS not only physically separate the chains of new neurons from the surrounding parenchyma, but also control neuronal migration by taking up GABA secreted from the migrating neurons (Bolteus and Bordey, 2004), releasing an activating factor (Mason et al., 2001), trapping vascular endothelial cell-derived BDNF (Snapyan et al., 2009), and expressing nonsoluble factors (Garcia-Marques et al., 2009). However, little is known about how the tubular astrocytic structures are maintained or how their interactions with migrating neurons are regulated.

Please cite this article in press as: Kaneko et al., New Neurons Clear the Path of Astrocytic Processes for Their Rapid Migration in the Adult Brain, Neuron (2010), doi:10.1016/j.neuron.2010.06.018

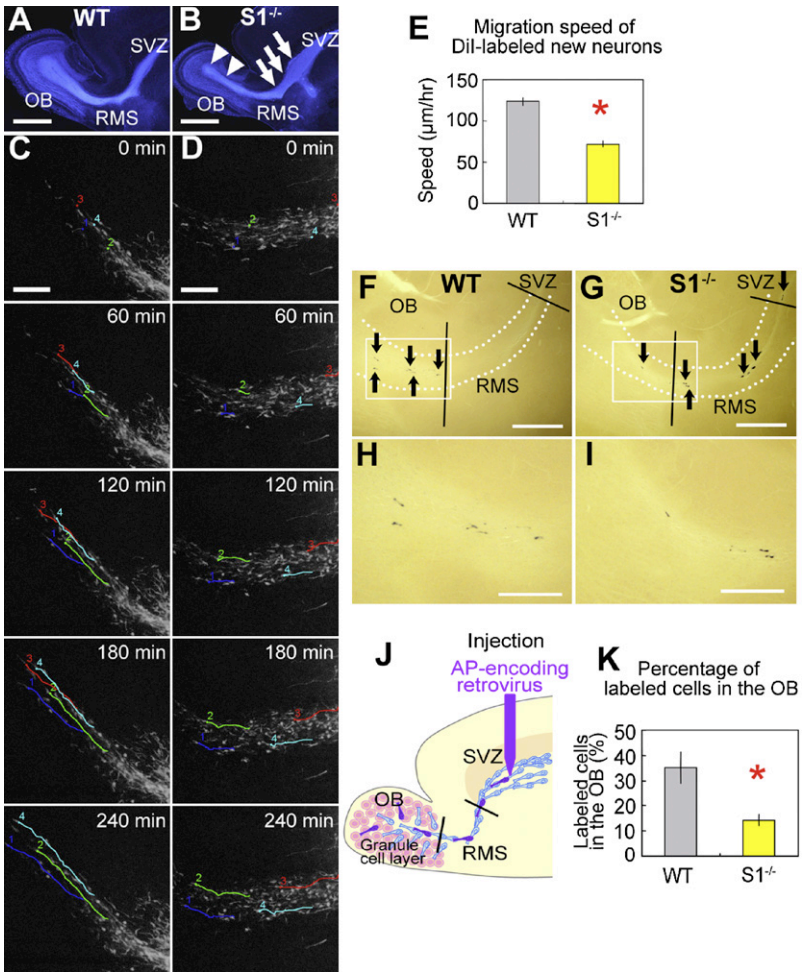

Figure 1. New Neuron Migration in the RMS of *S1*$^{-/-}$ Mice

(A and B) Hoechst-stained sagittal brain sections including the RMS of P7 WT (A) and *S1*$^{-/-}$ (B) mice. In the *S1*$^{-/-}$ brain, cells accumulated within the anterior part of the SVZ and proximal part of the RMS (arrows), whereas the distal part of the RMS and its extension inside the OB (arrowheads) were thinned.

(C–E) Time-lapse sequence of DiI-labeled cells migrating in the RMS of WT (C) and *S1*$^{-/-}$ (D) brain slices (OB is to left). Four cells in each slice are labeled (1, blue; 2, light green; 3, red; 4, cyan) in the 0 min panel, and their tracks over time are indicated by lines of the same color. The mean migration speed of DiI-labeled cells in the *S1*$^{-/-}$ RMS (yellow bar) was significantly slower than in the WT RMS (gray bar) (E, $p < 0.0001$).

(F–K) AP staining of WT (F) and *S1*$^{-/-}$ (G) brains 3 days after AP-encoding retroviral injection into the anterior SVZ (J). Arrows in (F) and (G) indicate AP-labeled migrating new neurons in the SVZ-RMS-OB pathway (between broken lines). Black lines indicate the boundaries of the SVZ, RMS, and OB. (H) and (I) are higher-magnification images of the boxes in (F) and (G), respectively. The percentage of AP-labeled cells inside the OB was significantly lower in the *S1*$^{-/-}$ than the WT brain (K, $p = 0.0011$). Error bars indicate ±SEM. Scale bars: 2 mm (A and B), 1 mm (F and G), 500 μm (H and I), 200 μm (C and D). See also Movie S1.

The Slit proteins, large diffusible proteins whose receptors are the Robo transmembrane proteins, guide extending axons and migrating neurons in the CNS through chemorepulsion (Andrews et al., 2006, 2007; Brose et al., 1999; Marín et al., 2003; Nguyen Ba-Charvet et al., 1999; Plump et al., 2002; Wu et al., 1999). Slit1 and Slit2 are expressed in periventricular tissue and repel new neurons (Hu, 1999; Hu and Rutishauser, 1996; Wu et al., 1999). Slit1 is also expressed by the neurons migrating in the SVZ-RMS-OB pathway, and it appears to have a cell-autonomous role in their migration (Nguyen-Ba-Charvet et al., 2004).

We show here an unexpected mechanism that the new neurons use to support their long-distance directional migration in the adult brain. Our results reveal that the RMS astrocytes express Robo receptors and respond to the repulsive activity of the neuron-secreted Slit by forming and maintaining glial tubes.

RESULTS

New Neuron Migration Is Disturbed in the RMS of *Slit1* Knockout Mice

We first examined the morphology of the mouse SVZ-RMS-OB pathway in Hoechst-stained sagittal sections (Figures 1A and 1B). In Slit1-deficient (*S1*$^{-/-}$) mice, the anterior part of the SVZ and proximal part of the RMS were thickened, whereas the distal (rostral) part of the RMS was thinned. We quantified the number of proliferating and apoptotic cells throughout the RMS pathway by labeling cells for BrdU incorporation and cleaved caspase-3, respectively. There were no significant differences in these values between the WT and *S1*$^{-/-}$ brains (BrdU: WT, 4440 ± 374 cells versus *S1*$^{-/-}$, 5296 ± 497 cells, $p = 0.231$; cleaved caspase-3: WT, 203 ± 44 cells versus *S1*$^{-/-}$, 242 ± 27 cells, $p = 0.434$), suggesting that the loss of Slit1 did not affect the proliferation or survival of the cells in this region. However, the new neurons apparently accumulated in the anterior SVZ and proximal RMS of the *S1*$^{-/-}$ mice.

To examine the migration defects of the new neurons in the *S1*$^{-/-}$ RMS, we compared their movement in *S1*$^{-/-}$ and WT brain slices in culture (Figures 1C–1E). To observe the migrating neurons, a DiI crystal was applied to the posterior part of the RMS in sagittal brain slices containing the SVZ-RMS-OB pathway. Time-lapse recordings of the DiI-labeled cells in the WT brain slices revealed that most neurons migrated rapidly along the RMS toward the OB, as previously reported (Murase and Horwitz, 2002). However, in slices prepared from *S1*$^{-/-}$ mice, the migration of the DiI-labeled cells was significantly slower (40% reduction in speed) (Figures 1C–1E and Movie S1).

To investigate the effects of the *Slit1* mutation on neuronal migration in vivo, we stereotaxically injected a recombinant retrovirus encoding alkaline phosphatase (AP) into the anterior part of the SVZ and counted the number of labeled cells in the SVZ, RMS, and OB 3 days later (Figures 1F–1K). There was no

Please cite this article in press as: Kaneko et al., New Neurons Clear the Path of Astrocytic Processes for Their Rapid Migration in the Adult Brain, Neuron (2010), doi:10.1016/j.neuron.2010.06.018

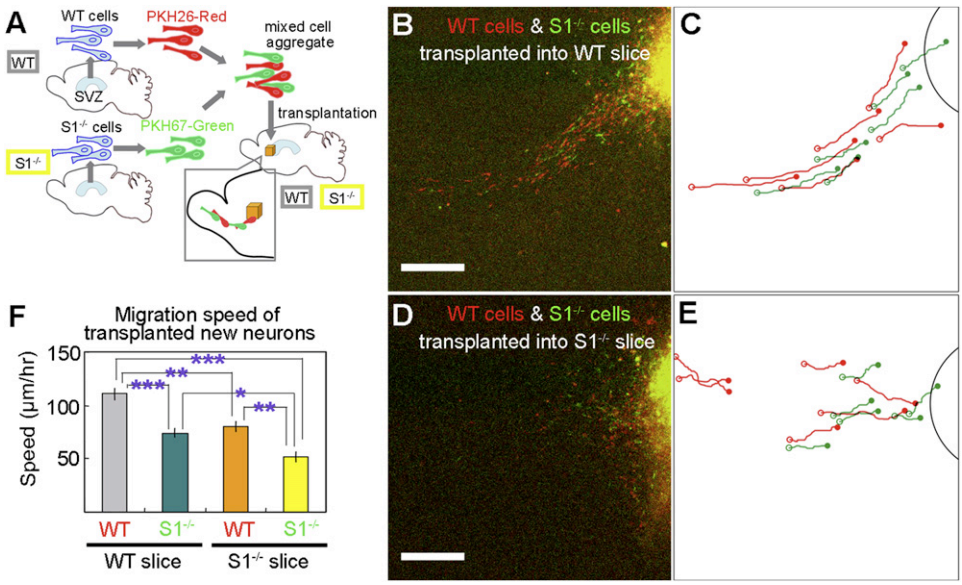

Figure 2. Migration of WT and S1 / Cells Transplanted into WT and S1 / Brain Slices

(A) Schematic drawing of the experimental protocol. New neurons dissociated from WT and *S1* / SVZs were labeled with different fluorescent dyes, red (PKH-26) for WT and green (PKH-67) for *S1* / , mixed into cell aggregates, and transplanted into the anterior SVZ of WT and *S1* / sagittal brain slices. The migration of the labeled cells was recorded by two-color time-lapse imaging.

(B–E) PKH-labeled transplanted WT (red) and *S1* / (green) cells migrating in a WT (B) or *S1* / (D) brain slice. Scale bars indicate 200 μm. OB is to the left. The cell tracks during 4 hr of monitoring are shown by the colored lines in (C) (WT) and (E) (*S1* /) (closed circles, cell positions at 0 min; open circles, positions at 240 min).

(F) Mean speed of migration of WT and *S1* / new neurons transplanted into WT (gray bar, WT cells; dark green bar, *S1* / cells) or *S1* / RMS (orange bar, WT cells; yellow bar, *S1* / cells). Compared with the speed of WT cells transplanted into WT slices, the speed of *S1* / cells transplanted into WT slices ($p < 0.0001$) and WT cells transplanted into *S1* / slices ($p = 0.0002$) was significantly reduced. The *S1* / cell migration speed was even slower in *S1* / slices (*S1* / cells in WT RMS versus *S1* / cells in *S1* / RMS: $p = 0.0041$, WT cells in *S1* / RMS versus *S1* / cells in *S1* / RMS: $p = 0.0007$). *$p < 0.05$, **$p < 0.01$, ***$p < 0.001$. Error bars indicate ±SEM. See also Movie S2.

significant difference in the total number of AP-labeled cells in the brains of the WT and *S1* / mice, indicating that Slit1 deficiency does not affect the infection or proliferation of the new neurons in the SVZ and RMS. However, the proportion of cells that reached the OB was significantly reduced in the *S1* / mice (Figure 1K). Together, these results clearly indicated that the migration of new neurons to the OB was disturbed in the *S1* / brain.

Efficient Migration through the RMS Requires Cell-Autonomous and Non-Cell-Autonomous Effects of Slit1 Expressed by the Migrating New Neurons

To examine whether it is necessary for a new neuron to express Slit1 for its own migration, we compared the migratory behavior of WT and *S1* / new neurons labeled with different fluorescent dyes (red for WT and green for *S1* /) in the RMS of WT brain slices, by two-color time-lapse recording (Figure 2). *S1* / cells transplanted into the *S1* / RMS (Figures 2D and 2E, green) showed slower migration than WT cells transplanted into the WT RMS (Figures 2B and 2C, red), similar to the cells labeled with DiI in the WT and *S1* / brain slices (Figures 1C and 1D). *S1* / new neurons migrating in the WT RMS also showed significantly slower speeds compared with Slit1-expressing WT cells (Figures 2B, 2C, and 2F). Thus, for rapid migration, the new neurons appeared to require Slit1 in a cell-autonomous manner. We next examined whether Slit1-expressing WT cells could migrate normally in a Slit1-deficient RMS (Figures 2D and 2E) by transplanting mixed aggregates of WT and *S1* / cells into a *S1* / brain slice. The WT cells in the *S1* / RMS (Figures 2D and 2E, red) showed slower and more irregular migration than those in the WT RMS (Figures 2B and 2C, red), suggesting that the normal migration of new neurons also required Slit1 expression by the surrounding new neurons (Movie S2).

We also tested whether the two dyes used in this experiment affected the new-neuron migration differently. WT cells were labeled with either the red or green fluorescent dye and transplanted into WT brain slices, but there were no significant differences in the migratory behaviors of the two groups of cells (data not shown).

Taken together, these results indicated that Slit1 derived from both the new neurons themselves and the surrounding new neurons in the RMS is necessary to regulate the migration of new neurons to the OB.

Robo Proteins Are Expressed in Migrating New Neurons and in the Surrounding Astrocytes in the RMS

We next sought to identify the cells expressing Slit's receptors, the Robo proteins, in the RMS. To compare the pattern of Robo expression with that of Slit1, brain sections of heterozygous *Slit1*-GFP knockin (Nguyen-Ba-Charvet et al., 2004; Plump et al., 2002) (Figure 3A) and WT (Figures 3B–3G) mice were stained using Robo1-, Robo2-, and Robo3-specific antibodies

Please cite this article in press as: Kaneko et al., New Neurons Clear the Path of Astrocytic Processes for Their Rapid Migration in the Adult Brain, Neuron (2010), doi:10.1016/j.neuron.2010.06.018

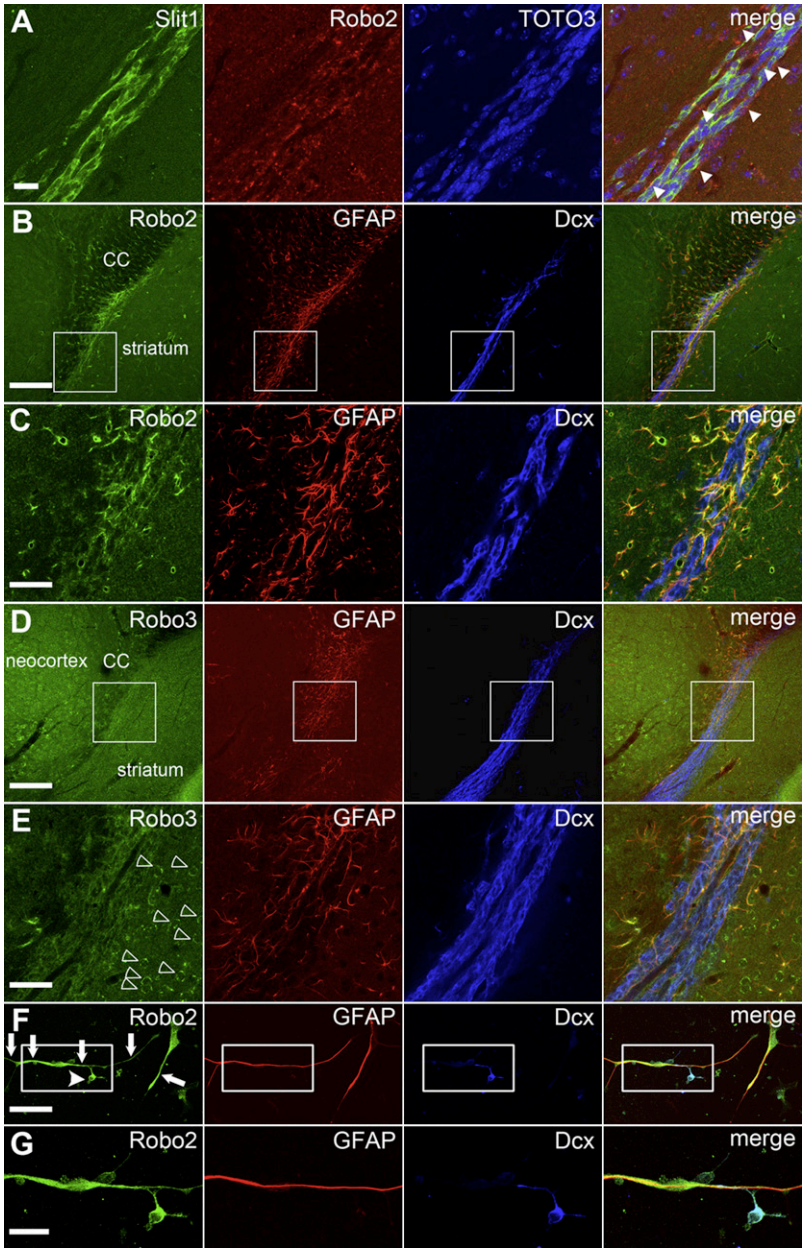

Figure 3. Localization of Robo2 Protein in the RMS

(A) Slit1/GFP and Robo2 immunohistochemistry in the RMS. Slit1/GFP (green) was localized to chain-forming new neurons in the RMS. Robo2 (red) protein was also detectable along the RMS, including in new neurons. Note that the Robo2+ processes with astrocytic morphology surrounding the chains of new neurons were negative for Slit1 (arrowheads). The nuclei were stained with TOTO3 (blue).

(B and C) Robo2 immunohistochemistry in the RMS. Robo2 protein (green) was detectable all along the RMS (B). High-magnification images. Boxed area in (B) shows that Robo2 (green) was strongly detected in the GFAP+ (red) astrocytic soma and processes and weakly in the Dcx+ (blue) new neurons (C).

(D and E) Robo3 immunohistochemistry in the RMS (E) is a high-magnification image of the boxed area in (D). Robo3 protein (green) was strongly detected in neurons in the neocortex and striatum (open arrowheads in E) and more weakly in the RMS. Within the RMS, the immunoreactivity of astrocytic processes (red) was easily detected, whereas that of new neurons (blue) was faint.

(F and G) Immunocytochemistry of cultured SVZ/RMS cells dissociated from adult WT mice. Robo2 (green) was localized to the GFAP+ (red) processes (arrows) and the soma of astrocytes, and to Dcx+ (blue) new neurons (arrowhead) (F). High-magnification images of the boxed area in (F) are shown in (G).

Scale bars: 200 μm (B and D), 50 μm (C, E, and F), 20 μm (A and G).

(Tamada et al., 2008). As previously reported (Nguyen-Ba-Charvet et al., 2004), the chain-forming new neurons in the SVZ and RMS expressed Slit1/GFP (green). They also expressed Robo2 (red), as expected (Long et al., 2007; Nguyen-Ba-Charvet et al., 2004). In addition, stronger Robo2 immunoreactivity was observed in Slit/GFP-negative cells in the RMS. Double immunostaining of Robo2 with cell-specific markers for new neurons (Dcx) and astrocytes (GFAP) showed that Robo2 was expressed strongly in the processes and soma of the astrocytes forming the glial tubes and weakly in the new neurons (Figures 3B and 3C). Furthermore, the astrocytic expression of Robo2 was observed almost exclusively in the SVZ-RMS-OB pathway and the corpus callosum overlying the SVZ and was undetectable in the hippocampus and neocortex (data not shown). Because it was difficult to distinguish the processes of new neurons from those of astrocytes in the RMS, where they were tightly associated, we confirmed the above expression pattern using dissociated SVZ cells plated on coverslips. We clearly observed Robo2 protein in the soma and processes of both astrocytes and new neurons (Figures 3F and 3G).

Consistent with a previous report on the localization of *Robo1* mRNA (Nguyen-Ba-Charvet et al., 2004), we did not detect Robo1 protein in the SVZ or RMS (data not shown). Robo3 was detected in the new neurons and astrocytes in the RMS, but its expression was stronger in the mature neurons of the neocortex and striatum (Figures 3D and 3E). In summary, the ligand Slit1 was expressed in the migrating new neurons, whereas its receptors Robo2 and Robo3 were expressed in both the new neurons and astrocytes. These expression patterns suggest that Slit-Robo signaling is involved in the interaction between new neurons and their surrounding astrocytes in the RMS and is not simply a directional cue for migrating neurons.

Cellular Organization of the RMS Is Disrupted in *S1*$^{-/-}$ Mice

To investigate whether Slit-Robo signaling affects the cellular organization of the RMS, sagittal and coronal sections of *S1*$^{-/-}$ and WT mouse brains were immunostained with antibodies to

Please cite this article in press as: Kaneko et al., New Neurons Clear the Path of Astrocytic Processes for Their Rapid Migration in the Adult Brain, Neuron (2010), doi:10.1016/j.neuron.2010.06.018

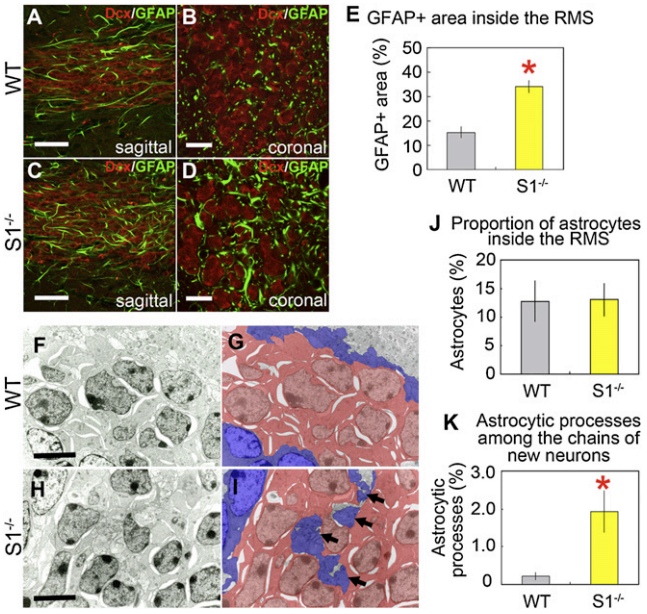

Figure 4. Cellular Organization of the RMS in *S1*$^{-/-}$ Mice

(A–E) Confocal images of the RMS of WT (A and B) and *S1*$^{-/-}$ (C and D) mice stained with Dcx (red) and GFAP (green). Sagittal sections of the WT RMS showed GFAP+ (green) astrocytic processes parallel to Dcx+ (red) new-neuron chains (A). The *S1*$^{-/-}$ RMS showed more, thick GFAP+ processes with irregular orientations, occasionally running across the chains (C). Coronal slices of WT RMS (B) showed cross-sections of thin GFAP+ astrocytic processes between clusters of Dcx+ neurons. The *S1*$^{-/-}$ RMS (D) showed many longitudinal sections of thick GFAP+ processes among the new neurons. Quantification of the GFAP+ area in the RMS showed that Slit1 deletion caused a significant increase in the amount of astrocytic processes within the RMS (E, $p = 0.0012$).

(F–K) Ultrastructural organization of the WT (F and G) and *S1*$^{-/-}$ (H and I) RMS, according to the criteria described in Experimental Procedures. New neurons (dark cytoplasm) and astrocytes (light cytoplasm) are indicated by red and blue, respectively (G and I). The percentage of astrocyte cell bodies in the RMS was not significantly different between the two groups (J, $p = 0.9558$); however, the astrocytic processes within chains were significantly more frequent in the *S1*$^{-/-}$ RMS (I, arrows) compared to controls (G). The area occupied by astrocytic processes inside the chains of new neurons was significantly increased in the *S1*$^{-/-}$ RMS (K, $p = 0.0409$).

Error bars indicate ±SEM. Scale bars: 50 μm (A and C), 20 μm (B and D), 5 μm (F–I). See also Figure S1.

GFAP and Dcx. Although new neurons accumulated in the *S1*$^{-/-}$ SVZ and RMS (Figure 1B), they still formed elongated chain-like aggregates, some of which were closely associated with adjacent blood vessels, much as in WT brains (Snapyan et al., 2009) (Figures S1A and S1B). However, the distribution and directionality of the astrocytic processes were altered in the *S1*$^{-/-}$ RMS (Figures 4A–4D). In the WT RMS, most of the astrocytic processes were oriented parallel to the chains of migrating new neurons. In contrast, irregular astrocytic processes were frequently observed running across the chains of new neurons in the *S1*$^{-/-}$ RMS. The proportion of the area inside the RMS occupied by GFAP+ processes in the *S1*$^{-/-}$ brains was more than twice that in the WT brains (Figure 4E).

To corroborate and extend this observation at higher resolution, we used electron microscopy. As described previously (Doetsch et al., 1997; Jankovski and Sotelo, 1996), the processes of astrocytes could be identified at the ultrastructural level by their light cytoplasm, which contained glycogen granules. They were readily distinguishable from the processes of new neurons in the RMS, which had a dark cytoplasm and contained many ribosomes (Figures 4F–4I). There was no significant difference in the percentage of astrocytic cell bodies among the identified cells in the RMS between the WT and *S1*$^{-/-}$ brains (Figure 4J). However, in the *S1*$^{-/-}$ RMS, astrocytic processes were observed within aggregates of new neurons. Such intermingling was rarely seen in the WT RMS (Figure 4K). The disorganization of glial tubes in the *S1*$^{-/-}$ RMS suggests that the Slit1 secreted by new neurons may facilitate their migration by actively preventing astrocytic processes from invading the migratory conduits within chains.

Slit Repels SVZ/RMS Astrocytes

The astrocytic expression of Robos (Figure 3) combined with the disorganization of the astrocytic tubes in Slit-deficient mice (Figure 4) strongly suggested that Slit can directly control the organization of astrocytes. To test this possibility, we performed an in vitro repulsion assay using a Slit-expressing HEK cell line (Wu et al., 1999) and primary cultured astrocytes dissociated from the SVZ and RMS. First, we examined the effect of Slit on the proliferation and survival of the astrocytes by culturing the astrocytes for 48 hr with conditioned medium from either Slit-expressing HEK cells or control, non-Slit-expressing HEK cells. The astrocytes were then double stained for GFAP and a mitotic cell marker, Ki67, or an apoptotic cell marker, cleaved caspase-3. There was no significant difference in the number of GFAP+ cells, i.e., astrocytes, or in the percentage of astrocytes expressing Ki67 or cleaved caspase-3 between the two culture conditions (data not shown), suggesting that Slit does not affect the proliferation or survival of SVZ/RMS astrocytes.

We next tested the effects of Slit on the migration of these astrocytes. For this purpose, the astrocytes were cocultured on plastic plates with small pieces of collagen gel containing Slit-expressing HEK cells or control HEK cells (Figures 5A–5C). After 4 days of culture, the distribution of astrocytes on the edges of the gel pieces was compared between the Slit and control groups. To quantify the GFAP+ cells, we measured the 500 μm wide strip just inside the edge of the gel piece and compared the GFAP+ area with the total area of the strip. Significantly fewer astrocytes lay on the Slit-containing gels than on the non-Slit-containing gels (Figures 5B–5D), suggesting that the astrocytes were repelled by Slit.

To investigate whether this repulsive effect of Slit was mediated by the Robo receptors expressed on the astrocytes, we used a dominant-negative form of Robo1 (Robo DN), which lacks the intracellular domains required for signal transduction (Hammond et al., 2005; Shiau et al., 2008) (Figures 5E–5K). The Robo DN-transfected SVZ/RMS astrocytes showed no significant change in proliferation, apoptosis, or Slit-independent migration activity compared with control astrocytes transfected with a vector encoding GFP (Figures S2A–S2I). However, compared with the controls (Figures 5F, 5G, and 5J), the Robo DN-transfected astrocytes were considerably less affected by Slit (Figures 5H, 5I, and 5K). Moreover, *Robo2* or *Robo3* knockdown

Please cite this article in press as: Kaneko et al., New Neurons Clear the Path of Astrocytic Processes for Their Rapid Migration in the Adult Brain, Neuron (2010), doi:10.1016/j.neuron.2010.06.018

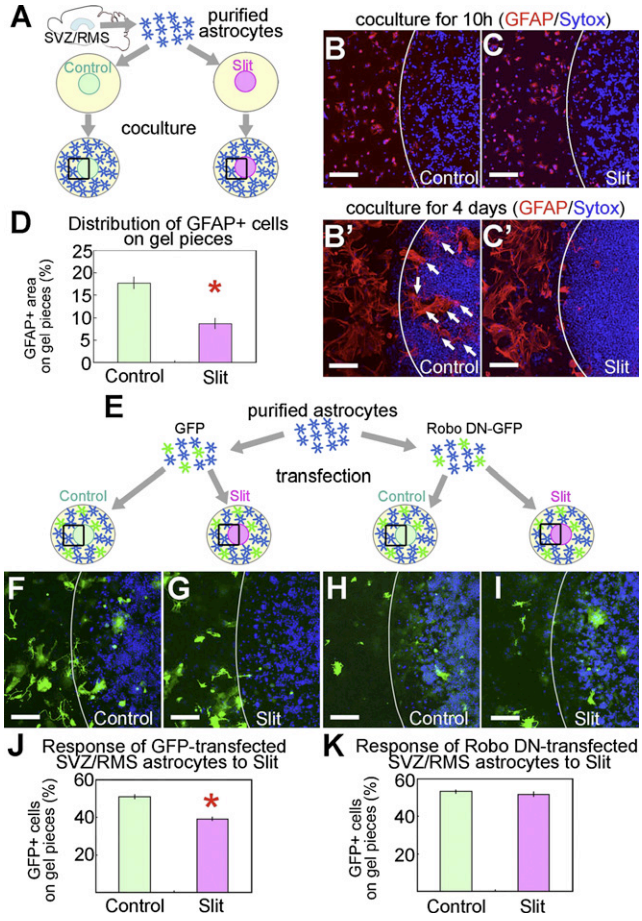

Figure 5. Repulsive Activity of Slit for Cultured Astrocytes

(A-D) SVZ/RMS astrocytes were cocultured with Slit-secreting (pink) and control (pale green) HEK cells mixed with collagen gel (A). Boxes in (A) indicate the magnified area shown in (B) and (C). After 10 hr, most astrocytes were attached to the dish and had short processes; few were on gel pieces containing control (B) or Slit-expressing (C) HEK cells. After 4 days, several astrocytes had migrated onto the pieces containing control HEK cells (B–B', arrows), but significantly fewer onto those containing Slit-secreting (C–C') HEK cells. The proportion of the 500 μm wide strip just inside the edge of the gel piece that was GFAP+ was quantified (D, $p = 0.0094$).

(E–K) Effects of Slit on astrocytes transfected with dominant-negative Robo (Robo DN). Cultured astrocytes dissociated from the SVZ and RMS were transfected with GFP-tagged Robo DN (H and I) or GFP (F and G), then cocultured with Slit-secreting or control HEK cells in collagen gel for 60 hr (E). Images show GFP+ cells near the edge of the control (F and H) and Slit-containing (G and I) HEK-cell-mixed gel. Graph shows the percentage of GFP+ GFAP+ astrocytes on the gel within 500 μm of its edge divided by the number in the 1000 μm wide space from 500 μm inside to 500 μm outside the gel border (J and K). The percentage of GFP-transfected astrocytes was significantly lower on Slit-containing gel pieces than on controls (J, $p = 0.0026$). This difference was not seen using astrocytes transfected with Robo DN-GFP (K).

Error bars indicate ±SEM. Scale bars: 200 μm. See also Figure S2.

by an shRNA-encoding lentivirus also suppressed the repulsive activity of Slit (Figures S2J–S2R), suggesting that Robo2 and Robo3 mediated the repulsion of the astrocytes by Slit, at least in part.

We further examined the possibility that neuronal Robos influences the arrangement of the astrocytes (Figures S2S–S2Z). To knock down the *Robo2* and *Robo3* specifically in new neurons, new neurons dissociated from a P0-2 mouse SVZ were infected with lentiviruses encoding either *Robo2* shRNA, *Robo3* shRNA, or a control sequence. The new neurons infected with each virus were then drop-cultured, mixed with astrocytes, and plated as aggregates on a laminin-coated dish. Twenty-four hours later, the new neurons had migrated out of the aggregates to a similar extent, regardless of the *Robo* knockdown or *Slit1* knockout (data not shown). Subsequently, the astrocytes began to extend their processes along the WT migrating new neurons (Figures S2S and S2T). Notably, the migration of *Slit1*$^{-/-}$ new neurons associated with astrocytes was significantly disturbed (Figures S2U and S2V). Consistent with our in vivo observation (Figures 4A–4D), the normal arrangement of the astrocytic processes was markedly disrupted when they were cocultured with Slit1-deficient new neurons (Figures S2U and S2V), further confirming our conclusion that neuronal Slit1 is required for the astrocytic arrangement. On the other hand, we did not observe any such disturbance in astrocytes cocultured with new neurons infected with lentiviruses encoding *Robo2* or *Robo3* shRNA (Figures S2W–S2Z). Taken together, these results suggest that the neuron-derived repulsive factor Slit1 and its receptors that are expressed on astrocytes, rather than on neurons, directly control the organization of the glial tube.

Newly Generated Neurons Control the Morphology of SVZ/RMS Astrocytes to Promote Their Own Migration

Finally, using new-neuron-astrocyte cocultures and time-lapse imaging, we studied the role of Slit-Robo signaling in the astrocytic control of neuronal migration and in the neuron-induced morphological changes in SVZ/RMS astrocytes. Aggregates of SVZ new neurons from WT or *S1*$^{-/-}$ mice were placed on plastic dishes with or without SVZ/RMS astrocytic feeder layers. On the dishes without astrocytes, there was no significant difference in the distance or speed of migration between *S1*$^{-/-}$ and WT new neurons (Figures 6A, 6B, 6E, S3A, S3D, and S3G). However, when *S1*$^{-/-}$ new neurons were plated on a monolayer of astrocytes, they migrated significantly more slowly than WT new neurons (Figures 6C, 6D, 6F, S3B, S3C, S3E, S3F, and S3H). This result suggested that Slit1$^{-/-}$'s promotion of neuronal migration depends on astrocytes.

To test whether the Slit1-expressing neurons directly induced morphological changes in astrocytes, we observed the astrocytes making contact with new neurons, by z-stack time-lapse imaging of genetically labeled new neurons (*Dcx-DsRed*; Wang et al., 2007) and astrocytes (*Gfap-EGFP*) cocultured in a 3D gel. Under these conditions, the cells were suspended and freely moving in 3D space, which better mimics the in vivo physical environment than does monolayer culture. Interestingly, furrows formed on the astrocytes' membrane where they contacted the migrating new neurons (arrows in Figures 7A–7C and Movie S3). To examine whether astrocytes making contact with new neurons displayed a similar morphology in vivo, we observed the 3D structure of the glial tubes surrounding the chains of new neurons by the confocal imaging of serial optical sections taken from the whole-mount SVZ. Using *Gfap-EGFP* mice, we

Please cite this article in press as: Kaneko et al., New Neurons Clear the Path of Astrocytic Processes for Their Rapid Migration in the Adult Brain, Neuron (2010), doi:10.1016/j.neuron.2010.06.018

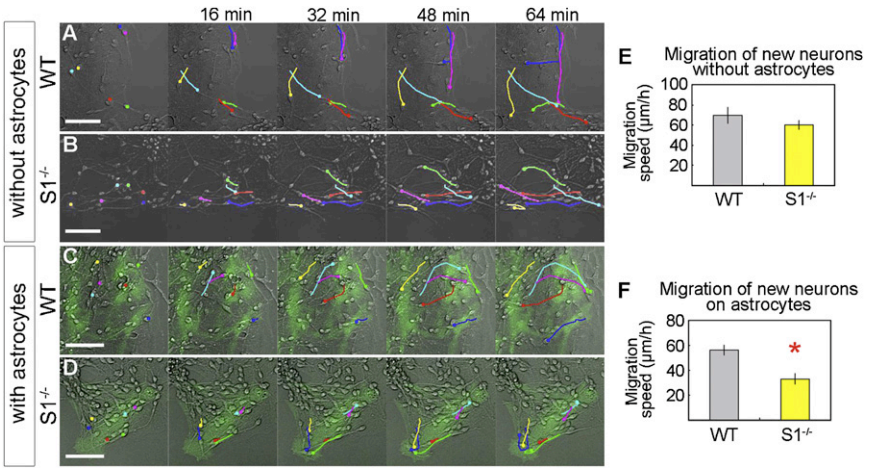

Figure 6. Slit1-Robo-Dependent Migration of New Neurons on Astrocytes

Migration speed of new neurons on an astrocytic feeder layer. Time-lapse sequence of WT (A) and *S1* $^{-/-}$ (B) new neurons migrating on the surface of plastic dishes without astrocytes. Representative tracks of the migrating new neurons indicated by dots and lines showed no significant difference in the migration speed between the two groups (E, p = 0.2850). Time-lapse sequence of WT (C) and *S1* $^{-/-}$ (D) new neurons migrating on astrocytes dissociated from the SVZ/RMS of *Gfap-EGFP* mice. The tracks of representative cells indicated by dots in the first panels are shown by lines in the following panels (16 min, 32 min, 48 min, 64 min). The migration speed of *S1* $^{-/-}$ new neurons on astrocytes was significantly reduced compared with that of WT new neurons (F, p = 0.0012). Error bars indicate ±SEM. Scale bars: 50 μm. See also Figure S3.

could visualize the morphology of the astrocytic membrane in contact with new neurons. The membrane of astrocytes formed clear invaginations with a size and shape that could accommodate the rounded outline of the chains of new neurons (Figure S4A), consistent with the observations in cultured cells (Movie S3). We further examined the fine morphology of the contact sites of the astrocyte membrane with new neurons by EM analyses. Close examination of coronal RMS sections revealed clear invaginations in the cell bodies of astrocytes along the contours of chain-forming new neurons (Figures S4B–S4E).

To determine whether these dynamic morphological changes were mediated by the Robo receptors on the astrocytes, aggregates of SVZ new neurons were placed on a monolayer of astrocytes transfected with either GFP-tagged Robo DN or GFP

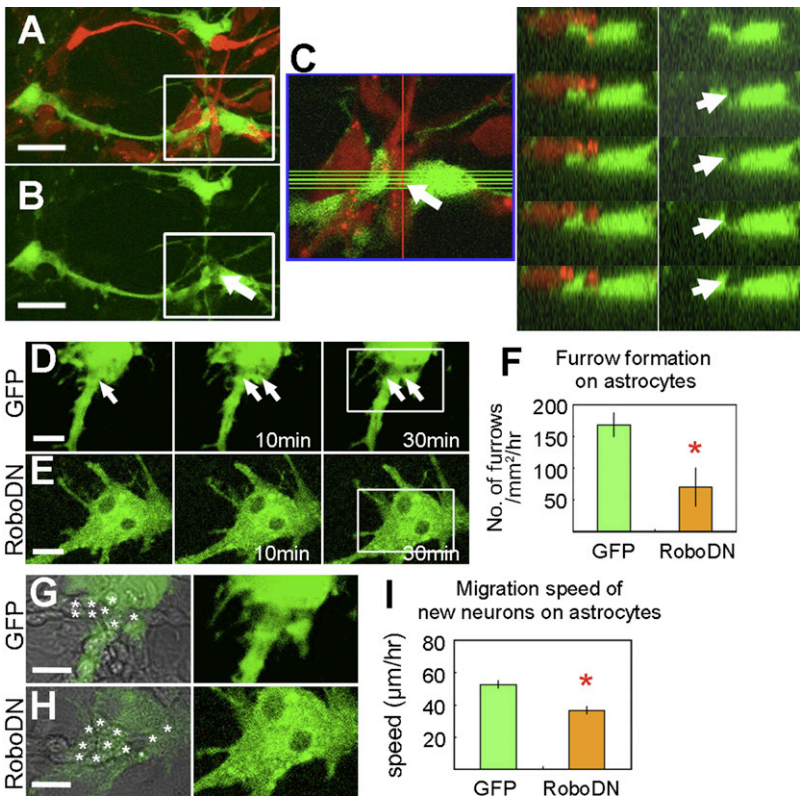

Figure 7. Dynamic Morphological Changes of Astrocytes Associated with Neuronal Migration

(A–C) New neurons (*Dcx-DsRed*) and SVZ/RMS astrocytes (*Gfap-EGFP*) were cocultured in 3D matrices (A). New neurons (red) migrated along the processes of astrocytes (green), on which furrows occasionally formed (B, arrows). A higher-magnification image of the boxed area in (A) is shown in (C). At right, a series of X-Z sections of the furrow on an astrocyte at the positions indicated by the green lines shown in the panel at left.

(D and E) Time-lapse recording of furrow formation. Middle and right panels show images captured 10 and 30 min after the left one. When new neurons migrated on a monolayer culture of SVZ/RMS astrocytes transfected with a control vector encoding GFP (D), the astrocytes changed their shape, occasionally forming furrows on the membrane in contact with the new neurons (arrows). Such morphological changes were suppressed in astrocytes transfected with dominant-negative Robo1 (Robo DN) (E).

(F) Quantification of the furrows. Graph shows the number of furrows formed on 1 mm^2 of the astrocyte membrane surface per hour, which was significantly reduced for astrocytes transfected with Robo DN compared with control-vector-transfected astrocytes (p = 0.0254).

(G and H) Higher-magnification images of the boxed regions in (D) and (E), respectively. The migration of new neurons (asterisks) over astrocytes was frequently associated with the formation of furrows on the membrane of astrocytes transfected with the control vector (G) but not with Robo DN (H).

(I) The migration speed of new neurons on Robo-DN-transfected astrocytes was significantly decreased compared with that on GFP-transfected astrocytes (p < 0.0001). Error bars indicate ±SEM. Scale bars: 20 μm. See also Figure S4 and Movies S3, S4, and S5.

Please cite this article in press as: Kaneko et al., New Neurons Clear the Path of Astrocytic Processes for Their Rapid Migration in the Adult Brain, Neuron (2010), doi:10.1016/j.neuron.2010.06.018

alone, and the morphology of these astrocytes was recorded. Similar furrows were formed on the membrane of both types of astrocytes where they contacted the migrating new neurons, but at a significantly lower frequency in the Robo DN-expressing astrocyte culture than in the control one (Figures 7D–7F and Movie S4). There was no significant difference in the spontaneous movement of the Robo DN-expressing and control astrocytes, suggesting that Robo DN does not affect general morphological changes in astrocytes that are not mediated by Slit-Robo signaling. New neurons from *S1*$^{-/-}$ mice induced similar furrows, but again at a significantly lower frequency than WT neurons (Figures S4F–S4H). These data suggested that the Slit secreted by migrating new neurons induces cell-shape changes in astrocytes through Robo signaling.

We then compared the speed of the new neurons migrating on Robo DN-expressing and control astrocytes. The mean migration speed of the new neurons on Robo DN-expressing astrocytes was significantly lower than on control astrocytes (Figures 7G–7I). Taken together, these results suggest that the Slit1 secreted by new neurons alters the morphology of astrocytes through the astrocytes' Robo receptors, thereby promoting the fast migration of new neurons in contact with the astrocytes.

DISCUSSION

Cell migration is controlled by extracellular cues within and near the cell's path. Here, we present evidence that the young neurons in the RMS of the adult brain help maintain an environment that is permissive for their own migration by actively modifying the astrocytic morphology.

In the embryonic neocortex, immature neurons are generated from precursors in the cortical ventricular zone and SVZ and migrate along radial glial fibers to populate the cortical plate (Hatten, 2002; Marín and Rubenstein, 2003; Miyata et al., 2001; Rakic, 1971; Rakic, 1972). The formation and maintenance of radial glia is partly controlled by signals from the migrating neurons (Anton et al., 1997; Schmid et al., 2003; Zheng et al., 1996), suggesting that the migrating neurons in the developing brain help regulate the morphology and function of cells along their migration route. However, the molecular mechanisms and dynamic anatomical changes used by the new neurons to regulate their migratory microenvironment have not been elucidated.

The postnatal brain offers unique opportunities for studying how young neurons regulate their migratory environment. Since the migratory routes are very long compared to those in the embryo, the migrating cells often have to navigate very complex territories, and migration is not a transitory phenomenon, but one that occurs throughout life. The long-distance migration of new neurons occurs in the SVZ-RMS-OB pathway in adult rodents and other mammals. Radial glia disappear within the first few postnatal days, and complex circuits of neuronal fibers and vasculature subsequently develop, accompanied by rapid increases in the numbers of other glial cells, including astrocytes. Therefore, new neurons in the adult brain migrate through densely packed tissue without the assistance of radial glia. Instead, SVZ-RMS new neurons migrate along one another, forming chains within glial tubes formed by astrocytes (Doetsch and Alvarez-Buylla, 1996; Jankovski and Sotelo, 1996; Lois et al., 1996; Wichterle et al., 1997). The glial tubes largely separate the chains of new neurons from the surrounding brain parenchyma, which helps to maintain the migration route. Genetic defects in glial tube formation have been reported, and these defects coincide with the abnormal migration of new neurons (Anton et al., 2004; Belvindrah et al., 2007; Chazal et al., 2000; Ghashghaei et al., 2006). However, the precise molecular interactions between SVZ-RMS migrating new neurons and their surrounding astrocytes have not been determined. Here, we showed that signaling between new neurons, which secrete Slit1 (Nguyen-Ba-Charvet et al., 2004), and astrocytes, which express Robo receptors, is critical for both the migration of new neurons and the formation and maintenance of the astrocytic tunnels.

The new neurons in *S1*$^{-/-}$ mice were reported to have defects in chain formation and directional migration in the SVZ and RMS (Nguyen-Ba-Charvet et al., 2004). Using time-lapse recording of migrating new neurons in the RMS of organotypic cultures and retroviral labeling of new neurons in vivo, we directly demonstrated that *S1*$^{-/-}$ new neurons migrate significantly more slowly than WT new neurons (Figure 1). We also showed that WT new neurons failed to migrate efficiently when placed in the RMS of a *S1*$^{-/-}$ brain (Figure 2). In the *S1*$^{-/-}$ brain, new neurons formed chains surrounded by glial tubes, but the morphology and arrangement of the astrocytic processes were significantly affected (Figure 4). These phenotypes suggested that Slit1 is involved in the formation and maintenance of glial structures that are permissive for normal long-range neuronal migration.

It is generally accepted that Slit proteins assist in the directional migration of new neurons born in the adult SVZ: Slit1 and Slit2 secreted from the choroid plexus and the septum direct neurons rostrally, toward the OB (Hu, 1999; Hu and Rutishauser, 1996; Sawamoto et al., 2006; Wu et al., 1999). Therefore, we expected that receptors for Slit would be expressed by the migrating new neurons. However, although the young neurons expressed low levels of the Robos, Robo2 and Robo3 were strongly expressed by the astrocytes forming the glial tubes (Figure 3), suggesting that the Slits might also play a role in organizing astrocytes along the migration route. Consistent with this possibility, inhibiting the Robo signal in astrocytes, but not in neurons, decreased Slit's effect on the morphology and arrangement of astrocytes (Figures 7 and S2S–S2Z). The knockout of *Slit1* or knockdown of *Robo* in new neurons cultured without astrocytes did not affect their migration (Figures 6, S2W–S2Z, S3A, S3D, and S3G). However, we cannot rule out the possibility that the absence of Slit1 directly affects the migration of new neurons, as previously reported (Nguyen-Ba-Charvet et al., 2004), because there are several methodological differences between our study and theirs. Instead, our results demonstrate a mechanism by which neuronal Slit1 affects astrocytes rather than new neurons in the formation and maintenance of glial structures that permit normal, long-range neuronal migration.

Using cultured astrocytes dissociated from the SVZ and RMS, we found that the Slits are a potential chemorepellent for SVZ/RMS astrocytes. Slits altered the distribution of astrocytes in the culture dish by a process that depended on the presence of Robo receptors (Figure 5). The endogenous Slit1 from new neurons did not completely "repel" the cell body of astrocytes,

possibly because the concentration of Slit1 produced by the new neurons was not high enough. Instead, the Slit1 expression by new neurons directly affected the distribution and extension of astrocytic processes in the RMS (Figure 4). Moreover, we demonstrated that the SVZ/RMS astrocytes underwent dynamic morphological changes that were dependent on Robo function and the association with migrating new neurons expressing Slit1 (Figures 6, 7, and S4F–S4H and Movie S4). The transient elimination of migrating neurons by the infusion of an antiproliferative drug, Ara-C, resulted in disrupted astrocytic morphology, followed by reorganization of the glial tubes during neuronal regeneration (Figures S4I–S4N). Furthermore we observed dynamic morphological changes of astrocytes in whole-mount SVZ cultures (Movie S5). Therefore, the glial tubes are not static but can be dynamically remodeled by new neurons migrating in vivo. The observation that WT young neurons failed to migrate normally when grafted into the RMS of *S1* $^{/}$ mice (Figure 2) also suggests that an increased Slit1 concentration, resulting from its secretion by collections of new neurons in chains, may be required to exclude astrocytic processes from the neurons' migratory canal. Thus, the facilitation of migration by Slit1 within the SVZ and RMS may require the collective secretion of Slit1 by migrating neurons. Our demonstration that migrating new neurons control the morphology of astrocytes could help explain how groups of new neurons that have coalesced into chains migrate through a corridor that is largely devoid of astrocytic processes.

In conclusion, we report an aspect of neuronal chain migration, in which new neurons actively control the cellular environment of their own migratory route. Such a mechanism is likely to be more significant physiologically in the migration of adult-born neurons than in the radial glia-guided neuronal migration of the embryonic brain.

EXPERIMENTAL PROCEDURES

Animals

Wild-type (WT) ICR mice were purchased from SLC (Shizuoka, Japan). The *Slit1* mutant mice and *Dcx-DsRed* transgenic mice were described previously (Plump et al., 2002; Wang et al., 2007). *Gfap-EGFP* mice were obtained from the Mutant Mouse Regional Resource Center. In accordance with the national regulations and guidelines, all experimental procedures were reviewed by the Institutional Laboratory Animal Care and Use Committee and approved by the President of Nagoya City University.

Time-Lapse Analyses of New Neurons Migrating in Brain Slices

Organotypic brain slices were prepared from P7–P8 mice as reported previously (Hirota et al., 2007; Murase and Horwitz, 2002; Suzuki and Goldman, 2003) with modifications. Dissected brains were cut into sagittal slices (325 μm thick), then cultured on a filter membrane (Millipore, Billerica, MA, USA) submerged in Neurobasal medium (Invitrogen, Carlsbad, CA) supplemented with 10% FBS, 2 mM L-glutamine, 2% B-27 (Invitrogen), and 50 U/ml penicillin-streptomycin. Before starting the time-lapse recording, a DiI crystal was applied to the posterior part of the RMS, and the slice was cultured for 8–13 hr in 5% CO_2 at 37 C. For the transplantation experiments, the dissected SVZ and RMS of P5-6 WT and *S1* $^{/}$ mice were dissociated using trypsin-EDTA (Invitrogen). The dissociated WT and *S1* $^{/}$ cells were labeled using the PKH-26 and PKH-67 Fluorescent Cell Linker Kit (Sigma, St. Louis, MO), respectively, reaggregated by centrifugation, cut into pieces (200 μm in diameter), and implanted into the posterior part of the RMS. The slices were cultured for 20–28 hr before recording.

Time-lapse video recordings were obtained using an inverted Zeiss confocal microscope LSM5 PASCAL (Carl Zeiss, Oberkochen, Germany) equipped with a stage top microscope incubator INU-ZI-F1 (5% CO_2 at 37 C, Tokai Hit, Shizuoka, Japan) using a 10× dry objective lens. Every 10 min, eight to ten optical Z sections (Z-steps: 8–12 μm) were obtained automatically over a period of 5 hr, and all of the focal planes were merged. The migration speed of the cells was quantified using NIH ImageJ version 1.38 software.

Histological Analysis

Animals were deeply anesthetized and perfused intracardially with 0.9% saline, followed by 4% paraformaldehyde (PFA) in 0.1 M phosphate buffer. The brain was extracted, postfixed in the same fixative overnight, and cut into 50 μm coronal or sagittal sections on a vibratome (VT1200S, Leica, Heidelberg, Germany).

For immunostaining, the sections were incubated for 1 hr in blocking solution (10% donkey serum and 0.2% Triton X-100 in PBS) overnight at 4 C with the primary antibodies, which were diluted in the same solution, and for 2 hr at room temperature with Alexa Fluor-conjugated secondary antibodies (Invitrogen). Signal amplification was performed with biotinylated secondary antibodies (Jackson Laboratory, West Grove, PA) and the Vectastain Elite ABC kit (Vector Laboratories, Burlingame, CA), and the signals were visualized using the TSA Fluorescence System (PerkinElmer, Waltham, MA) or diaminobenzidine tetrahydrochloride (DAB). For nuclear staining, Hoechst, SYTOX-orange, SYTOX-green, or TOTO3 iodide (Invitrogen) was used.

BrdU Labeling and Tissue Processing

BrdU (50 mg/kg body weight, dissolved in PBS) was intraperitoneally injected into 10- to 12-week-old mice. One hour later, the brain was fixed and processed into 50 μm coronal sections. Following incubation in 2 N HCl at 60 C for 30 min, the sections were incubated in PBS containing 1% H_2O_2, then immunostained with a rat anti-BrdU antibody (1:200, Abcam).

Quantification

The sections were examined using a confocal laser microscope (LSM5 Pascal, Zeiss) or fluorescence microscope (BX-51, Olympus, Tokyo, Japan). The number of immunoreactive cells was counted in every sixth coronal section (BrdU) or in serial sagittal sections (cleaved caspase-3), at a magnification of 400×.

To analyze the cytoarchitecture of the RMS, two coronal sections (550 μm apart) that had been immunostained with anti-Dcx and anti-GFAP antibodies were selected, and images of the horizontal limb of the bilateral RMS from both sections were captured by confocal laser microscopy (20× dry objective lens, Zeiss). The captured images were measured to determine the proportion of the GFAP+ area inside the RMS, using ImageJ software.

Electron Microscopic Analysis

Animals were deeply anesthetized and perfused intracardially with 30 ml of 0.9% saline followed by 100 ml of 2% PFA-2% glutaraldehyde in 0.1 M phosphate buffer. The brain was extracted, post-fixed with the same fixative overnight, and the RMS was cut into 500 μm coronal sections on a vibratome (VT1200S, Leica). The sections were postfixed with 2% OsO_4 in 0.1 M phosphate buffer for 2 hr, block-stained in 1% uranyl acetate, dehydrated with a graded series of alcohol, and embedded in Epon 812 (TAAB, Reading, UK). Silver sections were then cut with an ultramicrotome (Leica UC6; Leica Microsystems, Vienna, Austria), stained with uranyl acetate and lead citrate, and observed with an electron microscope (H-7100; Hitachi, Tokyo, Japan).

Electron micrographs of the chains of new neurons in the RMS of WT (n = 3) and *S1* $^{/}$ (n = 3) mice were taken at random with a primary magnification of ×4000. The images were printed on projection papers at 2.9 times the primary magnification. All analyses were performed within the core of the RMS. The contours and nuclei of all the cells included in an image were traced and classified as previously described (Doetsch and Alvarez-Buylla, 1996; Doetsch et al., 1997; Jankovski and Sotelo, 1996) into new neurons, astrocytes, and others. New neurons were identified by their very electron-dense nuclei and cytoplasm, whereas astrocytes were identified by their electron-lucent nuclei and cytoplasm and the presence of glycogen granules. To quantify the astrocytic processes inserted among the chains of new neurons, a double lattice

test system with a 1.5 cm spacing was used (Uchiyama and Watanabe, 1984). All of the points inside the chains of new neurons were classified as being on new neurons, astrocytes, other cells, or undetermined structures, then the percentage of points falling on astrocytes was calculated.

Retrovirus Microinjection and Tissue Processing

Each animal was given stereotaxic injections of 0.8 μl (0.1 μl at each of eight locations) of replication-incompetent retroviruses encoding the marker gene human placental alkaline phosphatase (DAP) harvested from the psi2 DAP cell line (American Type Cell Culture 1949-CRL) (Fields-Berry et al., 1992) into the anterior SVZ of each hemisphere. Three days later, the brains were fixed as described above, cut into 50 μm sagittal serial sections, and processed for alkaline phosphatase (AP) histochemistry as previously described (Fields-Berry et al., 1992). The number of retrovirus-infected AP-stained (AP+) cells in the SVZ, RMS, and OB, respectively, was counted under 200× magnification.

Culture of SVZ/RMS Astrocytes

The SVZ and RMS were dissected from postnatal day 10 (P10)–P12 WT or *Gfap-EGFP* mice in L-15 medium (Invitrogen) and dissociated with trypsin-EDTA (Invitrogen). The dissociated cells were washed with L-15 medium, plated, and cultured with DMEM containing 10% FBS, 50 U/ml penicillin-streptomycin, and 2 mM L-glutamine. To purify astrocytes from the mixed culture of SVZ/RMS tissue, the cells were replated three times at 3–4 day intervals, then incubated with shaking for 20 min before use.

Coculture of SVZ/RMS Astrocytes with Slit-Expressing Cells

Stably transfected HEK cell lines expressing the full-length *Xenopus* Slit protein, and control HEK cells transfected with the vector plasmid (Wu et al., 1999) were mixed with 2% collagen gel and plated as one 10 μl gel-cell aggregate in each well of 24-well plates. Following a 1 hr incubation to polymerize the cell-containing gel, the gel pieces were cultured with DMEM medium containing 2% FBS and 50 U/ml penicillin-streptomycin overnight. Cultured SVZ/RMS astrocytes were resuspended in the same medium, plated into the same dish as the gel piece, and cultured at 37 C in a 5% CO_2 incubator. Seventy hours later, the cells were fixed with 4% PFA in 0.1 M phosphate buffer and immunostained with an anti-GFAP antibody. The distribution of GFAP+ cells on the gel pieces (within 500 μm of the edge) containing Slit-expressing cells and control cells were compared as follows: the merged images of nine optical Z-sections of the area at 5 μm intervals were obtained by confocal laser microscopy (10× dry objective lens, LSM5 PASCAL, Zeiss). The area that was GFAP+ in the 500 μm wide strip just inside the edge of the gel piece was determined using NIH ImageJ software.

Transfection of a Dominant-Negative Form of Robo

Cultured astrocytes were transfected with a plasmid encoding either a GFP-tagged dominant-negative form of Robo1 (Robo DN) or GFP (control) using Lipofectamine LTX Plus reagent (Invitrogen), three times at 12 hr intervals. Twelve hours after the final transfection, the cells were plated as described above, and then cultured for 60 hr before fixation.

Migration of New Neurons Associated with Cultured SVZ/RMS Astrocytes

The SVZ was dissected from P0-2 WT and *S1*$^{-/-}$ mice, the cells were dissociated and reaggregated, and the aggregates were cut into pieces (150–200 μm in diameter), as described above. The pieces of WT and *S1*$^{-/-}$ cells were plated on laminin-coated dishes or on monolayer cultures of SVZ/RMS astrocytes transfected with Robo DN or control vector (GFP), from WT or *Gfap-EGFP* mice and cultured for 24–36 hr, before imaging. The migration behavior of new neurons and their interaction with astrocytes were recorded by time-lapse imaging at 6 or 8 min intervals for 3–5 hr using confocal microscopy. The tracks of continuously migrating cells with the typical morphology of new neurons that could be traced for more than 40 min were used to calculate the migration speed in each situation.

To observe the furrow formation on astrocytes in 3D culture, the aggregates of SVZ cells dissociated from *Dcx-DsRed* mice were embedded into Matrigel in which SVZ/RMS astrocytes from *Gfap-EGFP* mice were suspended. After 24 hr of culture, time-lapse images were automatically captured by a confocal laser microscope (LSM710, Zeiss), every 2 min as 20 optical Z sections (Z-steps: 1 μm), for 3 hr.

Statistical Analysis

All data were expressed as the mean ± standard error of the mean (SEM). Differences between means were determined by two-tailed Student's t test or one-way ANOVA followed by a Tukey-Kramer multiple comparison test. A p value of <0.05 was considered significant.

SUPPLEMENTAL INFORMATION

Supplemental Information includes four figures, five movies, and Supplemental Experimental Procedures and can be found with this article online at doi:10.1016/j.neuron.2010.06.018.

ACKNOWLEDGMENTS

We thank the anonymous reviewers for helpful comments on the manuscript; Dr. Fujio Murakami for providing the specific antibodies to Robo1 and Robo2; Dr. Didier Trono for providing the lentivirus packaging plasmids, psPAX2 and pMD2.G; Dr. Nathaniel Heintz and the Mutant Mouse Regional Resource Center (MMRRC) for providing the Gfap-EGFP mice; and Drs. Ichiro Miyoshi, Tatsumi Hirata, Francois Renault-Mihara and Takehiko Sunabori and Miss Rie Ueda for technical support. This work was supported by research grants from the Ministry of Education, Culture, Sports, Science & Technology (MEXT), Ministry of Health, Labor and Welfare (MHLW), Japan Society for the Promotion of Science (JSPS), Human Frontier Science Program (HFSP), Toray Science Foundation, Keio University Medical Science Fund, Inoue Foundation for Science, NOVARTIS Foundation (Japan) for the Promotion of Science, and Kowa Life Science Foundation. J.Y.W is supported by NIH (CA114197, CA107193) and James S. McDonnell Foundation. N.K. was an Inoue Fellow.

Accepted: June 8, 2010
Published: July 28, 2010

REFERENCES

Andrews, W., Liapi, A., Plachez, C., Camurri, L., Zhang, J., Mori, S., Murakami, F., Parnavelas, J.G., Sundaresan, V., and Richards, L.J. (2006). Robo1 regulates the development of major axon tracts and interneuron migration in the forebrain. Development *133*, 2243–2252.

Andrews, W.D., Barber, M., and Parnavelas, J.G. (2007). Slit-Robo interactions during cortical development. J. Anat. *211*, 188–198.

Anton, E.S., Marchionni, M.A., Lee, K.F., and Rakic, P. (1997). Role of GGF/neuregulin signaling in interactions between migrating neurons and radial glia in the developing cerebral cortex. Development *124*, 3501–3510.

Anton, E.S., Ghashghaei, H.T., Weber, J.L., McCann, C., Fischer, T.M., Cheung, I.D., Gassmann, M., Messing, A., Klein, R., Schwab, M.H., et al. (2004). Receptor tyrosine kinase ErbB4 modulates neuroblast migration and placement in the adult forebrain. Nat. Neurosci. *7*, 1319–1328.

Belvindrah, R., Hankel, S., Walker, J., Patton, B.L., and Müller, U. (2007). Beta1 integrins control the formation of cell chains in the adult rostral migratory stream. J. Neurosci. *27*, 2704–2717.

Bolteus, A.J., and Bordey, A. (2004). GABA release and uptake regulate neuronal precursor migration in the postnatal subventricular zone. J. Neurosci. *24*, 7623–7631.

Brose, K., Bland, K.S., Wang, K.H., Arnott, D., Henzel, W., Goodman, C.S., Tessier-Lavigne, M., and Kidd, T. (1999). Slit proteins bind Robo receptors and have an evolutionarily conserved role in repulsive axon guidance. Cell *96*, 795–806.

Chazal, G., Durbec, P., Jankovski, A., Rougon, G., and Cremer, H. (2000). Consequences of neural cell adhesion molecule deficiency on cell migration in the rostral migratory stream of the mouse. J. Neurosci. *20*, 1446–1457.

Doetsch, F., and Alvarez-Buylla, A. (1996). Network of tangential pathways for neuronal migration in adult mammalian brain. Proc. Natl. Acad. Sci. USA *93*, 14895–14900.

Doetsch, F., García-Verdugo, J.M., and Alvarez-Buylla, A. (1997). Cellular composition and three-dimensional organization of the subventricular germinal zone in the adult mammalian brain. J. Neurosci. *17*, 5046–5061.

Fields-Berry, S.C., Halliday, A.L., and Cepko, C.L. (1992). A recombinant retrovirus encoding alkaline phosphatase confirms clonal boundary assignment in lineage analysis of murine retina. Proc. Natl. Acad. Sci. USA *89*, 693–697.

Garcia-Marques, J., De Carlos, J.A., Greer, C.A., and Lopez-Mascaraque, L. (2009). Different astroglia permissivity controls the migration of olfactory bulb interneuron precursors. Glia *58*, 218–230.

Ghashghaei, H.T., Weber, J., Pevny, L., Schmid, R., Schwab, M.H., Lloyd, K.C., Eisenstat, D.D., Lai, C., and Anton, E.S. (2006). The role of neuregulin-ErbB4 interactions on the proliferation and organization of cells in the subventricular zone. Proc. Natl. Acad. Sci. USA *103*, 1930–1935.

Hammond, R., Vivancos, V., Naeem, A., Chilton, J., Mambetisaeva, E., Mambitisaeva, E., Andrews, W., Sundaresan, V., and Guthrie, S. (2005). Slit-mediated repulsion is a key regulator of motor axon pathfinding in the hindbrain. Development *132*, 4483–4495.

Hatten, M.E. (2002). New directions in neuronal migration. Science *297*, 1660–1663.

Hirota, Y., Ohshima, T., Kaneko, N., Ikeda, M., Iwasato, T., Kulkarni, A.B., Mikoshiba, K., Okano, H., and Sawamoto, K. (2007). Cyclin-dependent kinase 5 is required for control of neuroblast migration in the postnatal subventricular zone. J. Neurosci. *27*, 12829–12838.

Hu, H. (1999). Chemorepulsion of neuronal migration by Slit2 in the developing mammalian forebrain. Neuron *23*, 703–711.

Hu, H., and Rutishauser, U. (1996). A septum-derived chemorepulsive factor for migrating olfactory interneuron precursors. Neuron *16*, 933–940.

Jankovski, A., and Sotelo, C. (1996). Subventricular zone-olfactory bulb migratory pathway in the adult mouse: cellular composition and specificity as determined by heterochronic and heterotopic transplantation. J. Comp. Neurol. *371*, 376–396.

Kaneko, N., and Sawamoto, K. (2009). Adult neurogenesis and its alteration under pathological conditions. Neurosci. Res. *63*, 155–164.

Lois, C., and Alvarez-Buylla, A. (1994). Long-distance neuronal migration in the adult mammalian brain. Science *264*, 1145–1148.

Lois, C., García-Verdugo, J.M., and Alvarez-Buylla, A. (1996). Chain migration of neuronal precursors. Science *271*, 978–981.

Long, J.E., Garel, S., Alvarez-Dolado, M., Yoshikawa, K., Osumi, N., Alvarez-Buylla, A., and Rubenstein, J.L. (2007). Dlx-dependent and -independent regulation of olfactory bulb interneuron differentiation. J. Neurosci. *27*, 3230–3243.

Marín, O., and Rubenstein, J.L. (2003). Cell migration in the forebrain. Annu. Rev. Neurosci. *26*, 441–483.

Marín, O., Plump, A.S., Flames, N., Sánchez-Camacho, C., Tessier-Lavigne, M., and Rubenstein, J.L. (2003). Directional guidance of interneuron migration to the cerebral cortex relies on subcortical Slit1/2-independent repulsion and cortical attraction. Development *130*, 1889–1901.

Mason, H.A., Ito, S., and Corfas, G. (2001). Extracellular signals that regulate the tangential migration of olfactory bulb neuronal precursors: inducers, inhibitors, and repellents. J. Neurosci. *21*, 7654–7663.

Miyata, T., Kawaguchi, A., Okano, H., and Ogawa, M. (2001). Asymmetric inheritance of radial glial fibers by cortical neurons. Neuron *31*, 727–741.

Murase, S., and Horwitz, A.F. (2002). Deleted in colorectal carcinoma and differentially expressed integrins mediate the directional migration of neural precursors in the rostral migratory stream. J. Neurosci. *22*, 3568–3579.

Nguyen Ba-Charvet, K.T., Brose, K., Marillat, V., Kidd, T., Goodman, C.S., Tessier-Lavigne, M., Sotelo, C., and Chédotal, A. (1999). Slit2-Mediated chemorepulsion and collapse of developing forebrain axons. Neuron *22*, 463–473.

Nguyen-Ba-Charvet, K.T., Picard-Riera, N., Tessier-Lavigne, M., Baron-Van Evercooren, A., Sotelo, C., and Chédotal, A. (2004). Multiple roles for slits in the control of cell migration in the rostral migratory stream. J. Neurosci. *24*, 1497–1506.

Okano, H., and Sawamoto, K. (2008). Neural stem cells: involvement in adult neurogenesis and CNS repair. Philos. Trans. R. Soc. Lond. B Biol. Sci. *363*, 2111–2122.

Petreanu, L., and Alvarez-Buylla, A. (2002). Maturation and death of adult-born olfactory bulb granule neurons: role of olfaction. J. Neurosci. *22*, 6106–6113.

Plump, A.S., Erskine, L., Sabatier, C., Brose, K., Epstein, C.J., Goodman, C.S., Mason, C.A., and Tessier-Lavigne, M. (2002). Slit1 and Slit2 cooperate to prevent premature midline crossing of retinal axons in the mouse visual system. Neuron *33*, 219–232.

Rakic, P. (1971). Guidance of neurons migrating to the fetal monkey neocortex. Brain Res. *33*, 471–476.

Rakic, P. (1972). Mode of cell migration to the superficial layers of fetal monkey neocortex. J. Comp. Neurol. *145*, 61–83.

Sawamoto, K., Wichterle, H., Gonzalez-Perez, O., Cholfin, J.A., Yamada, M., Spassky, N., Murcia, N.S., Garcia-Verdugo, J.M., Marin, O., Rubenstein, J.L., et al. (2006). New neurons follow the flow of cerebrospinal fluid in the adult brain. Science *311*, 629–632.

Schmid, R.S., McGrath, B., Berechid, B.E., Boyles, B., Marchionni, M., Sestan, N., and Anton, E.S. (2003). Neuregulin 1-erbB2 signaling is required for the establishment of radial glia and their transformation into astrocytes in cerebral cortex. Proc. Natl. Acad. Sci. USA *100*, 4251–4256.

Shiau, C.E., Lwigale, P.Y., Das, R.M., Wilson, S.A., and Bronner-Fraser, M. (2008). Robo2-Slit1 dependent cell-cell interactions mediate assembly of the trigeminal ganglion. Nat. Neurosci. *11*, 269–276.

Snapyan, M., Lemasson, M., Brill, M.S., Blais, M., Massouh, M., Ninkovic, J., Gravel, C., Berthod, F., Götz, M., Barker, P.A., et al. (2009). Vasculature guides migrating neuronal precursors in the adult mammalian forebrain via brain-derived neurotrophic factor signaling. J. Neurosci. *29*, 4172–4188.

Suzuki, S.O., and Goldman, J.E. (2003). Multiple cell populations in the early postnatal subventricular zone take distinct migratory pathways: a dynamic study of glial and neuronal progenitor migration. J. Neurosci. *23*, 4240–4250.

Tamada, A., Kumada, T., Zhu, Y., Matsumoto, T., Hatanaka, Y., Muguruma, K., Chen, Z., Tanabe, Y., Torigoe, M., Yamauchi, K., et al. (2008). Crucial roles of Robo proteins in midline crossing of cerebellofugal axons and lack of their up-regulation after midline crossing. Neural Dev. *3*, 29.

Uchiyama, Y., and Watanabe, M. (1984). A morphometric study of developing pancreatic acinar cells of rats during prenatal life. Cell Tissue Res. *237*, 117–122.

Wang, X., Qiu, R., Tsark, W., and Lu, Q. (2007). Rapid promoter analysis in developing mouse brain and genetic labeling of young neurons by doublecortin-DsRed-express. J. Neurosci. Res. *85*, 3567–3573.

Wichterle, H., Garcia-Verdugo, J.M., and Alvarez-Buylla, A. (1997). Direct evidence for homotypic, glia-independent neuronal migration. Neuron *18*, 779–791.

Wu, W., Wong, K., Chen, J., Jiang, Z., Dupuis, S., Wu, J.Y., and Rao, Y. (1999). Directional guidance of neuronal migration in the olfactory system by the protein Slit. Nature *400*, 331–336.

Zheng, C., Heintz, N., and Hatten, M.E. (1996). CNS gene encoding astrotactin, which supports neuronal migration along glial fibers. Science *272*, 417–419.